2. Theory

2.1. Decorrelated parametric down-conversion

The spectral properties of a PDC process in waveguides are governed by the energy and momentum conservation laws

$$\omega_s + \omega_i = \omega_p, \qquad k_s + k_i + \frac{2\pi}{\Lambda} = k_p, \tag{1}$$

where ω is the frequency of the signal, idler or pump photons, respectively, k their propagation constant and Λ the period of a periodic poling of the waveguide. Energy and momentum are linked by the dispersion relation $\omega(k)$ of the waveguide, mainly influenced by the material properties. For short pump pulses, a distribution of frequencies has to be taken into account, the pump function $\alpha(\omega_p)$. Similarly, for waveguides of finite lengths, the momentum conservation is described by a phasematching function $\phi(\omega_s, \omega_i)$. The full process is then described by the joint spectral amplitude (JSA)

$$f(\omega_s, \omega_i) = \phi(\omega_s, \omega_i)\alpha(\omega_s, \omega_i) \tag{2}$$

and the Hamiltonian is given by $H = \zeta \int \int d\omega_s d\omega_i f(\omega_s, \omega_i) a_s^\dagger(\omega_s) a_i^\dagger(\omega_i) + \text{h.c.}$, where $a^\dagger(\omega)$ is the standard creation operator at frequency ω. The amount of spectral correlations can be quantified by the Schmidt number $K = 1/\sum_k |c_k|^4$, where the coefficients c_k result from the Schmidt decomposition of the JSA: $f(\omega_s, \omega_i) = \sum_k c_k \phi_k(\omega_s)\psi_k(\omega_i)$, with orthonormal functions ϕ_k and ψ_k [24]. In particular for $K = 1$, signal and idler are decorrelated and the state is separable.

Most PDC sources exhibit a negatively correlated phasematching function $\phi(\omega_s, \omega_i)$. Since the pump function $\alpha(\omega_s, \omega_i)$ is always oriented exactly at $-45°$ due to energy conservation, spectral correlations cannot be avoided in these sources. With a positively oriented phasematching, however, spectral decorrelation is possible. By dispersion engineering, i.e. choosing the right material, and adjustment of the pump width, spectral decorrelation can be achieved [13]. KTP waveguides have a phasematching correlation angle of approximately $59°$ [25] at telecom wavelengths around 1550 nm. Assuming a Gaussian pump spectrum and a Gaussian phasematching function, which is a good approximation for realistic, slightly inhomogeneous waveguides, the joint spectral amplitude becomes perfectly separable with a shape that is close to round, see Fig. 1.
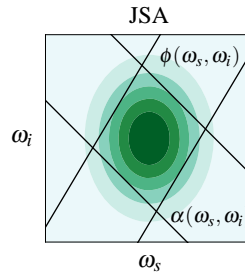

Fig. 1. Separable joint spectral amplitude resulting from a phasematching function ϕ with a positive slope multiplied by a pump function α of appropriate width.

2.2. Source characterization

Hong Ou Mandel interference between signal and idler   The interference of twin photons at a beamsplitter followed by a coincidence measurement with single photon detectors is a well

established method to deduce information about a biphoton quantum state. First demonstrated by Hong, Ou and Mandel [26] to measure the duration of photon wavepackets, it can be used as a measure of indistinguishability [6,27,28] and even for reconstruction of the spectral properties of a state [29–31]. The Hong-Ou-Mandel (HOM) interference is unaffected by loss and has been widely applied for the characterization of single photon states from PDC.

Assuming that signal and idler originate from a perfect, weakly pumped PDC source with a not necessarily decorrelated JSA $f(\omega_s, \omega_i)$, the probability of a coincidence click after the interference at a 50/50 beam splitter for a time delay τ between signal and idler is given by

$$p(\tau) = \frac{1}{2} - \frac{1}{2}\mathrm{Re}\int d\omega_s d\omega_i f^*(\omega_s, \omega_i) f(\omega_i, \omega_s) e^{-i\tau(\omega_s - \omega_i)}. \qquad (3)$$

For $\tau = 0$, the integral term is the overlap between the JSA and its mirrored counterpart along the 45° line. A HOM measurement hence probes the symmetry of the state under the exchange of signal and idler, as illustrated in Fig. 2.
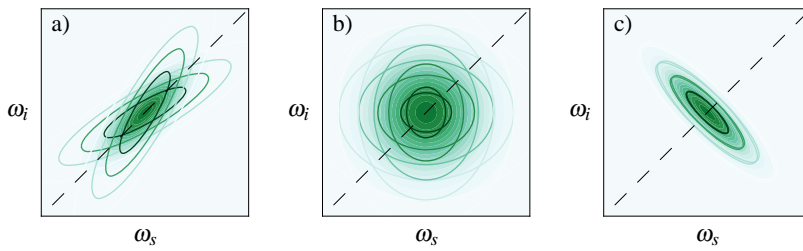

Fig. 2. The visibility of the HOM interference is proportional to the overlap (shaded area) of the JSA with itself under the exchange of signal and idler (contour plots). a) Positive correlation, $K = 2$ and visibility 70%. b) Decorrelation, $K = 1$ and visibility 96.7%. c) Negative correlation, $K = 2$ and visibility 99.8%. Panel b) corresponds to the situation presented in this paper.

Hong Ou Mandel interference with a reference field For the phasematching correlation angle of our source, high visibilities in a HOM interference between signal and idler can be obtained in the decorrelated as well as in the negatively correlated case. Our goal, however, is to produce decorrelated states as in the central plot of Fig. 2. To distinguish between the decorrelated and the correlated case, it is necessary to interfere the state with an independent reference beam. This can be understood as a purity measurement of the marginal beams.

If signal and idler are correlated, tracing out the idler mode results in a mixed signal state, described in frequency space by a density matrix $\rho_s(\omega_s, \omega'_s)$. Being hermitian, this matrix must be symmetric with respect to the principal diagonal. In the following we assume that it is a 2-dimensional Gaussian function, which is well justified for our source as discussed in Sec. 3.2. It follows from straight forward calculations that the purity of the state is given by $\mathrm{Tr}(\rho_s^2) = \sigma_2/\sigma_1$, where σ_1 and σ_2 are the major and minor axes of the Gaussian function $\rho_s(\omega_s, \omega'_s)$. The major axis is the spectral width of the signal beam and can be measured directly with a spectrometer. The minor axis cannot be accessed directly with a spectral measurement but has an influence on the coherence length of the state and hence the interference pattern, as depicted in Fig. 3. By a HOM interference measurement with a known reference field, the minor axis can be deduced from the temporal width of the HOM dip, which is given by

$$\delta^2 = \frac{1}{2\sigma_2^2} + \frac{1}{2\sigma_\beta^2} \qquad (4)$$

where σ_β is the width of the reference field. A detailed analysis of this technique can be found in [32]. Note that a measurement of the widths is much more robust compared to a measurement of the visibility because it is not affected by higher photon number components and imperfect overlaps of the state in the spectral and polarization degree of freedom. For comparison with the JSA, the relation between the purity and the Schmidt number is simply given by $P = 1/K$.
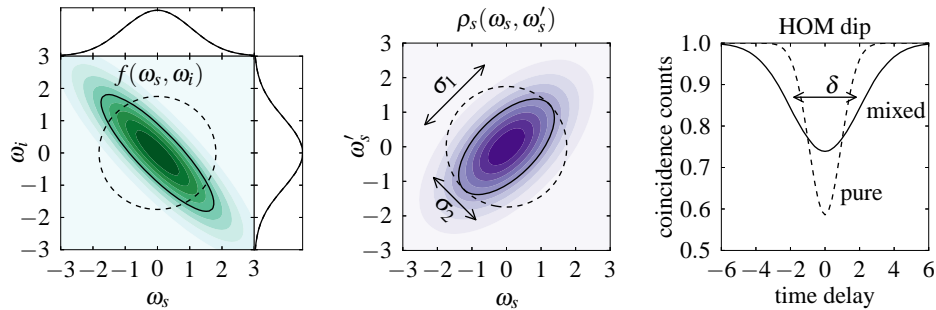

Fig. 3. Comparison of an uncorrelated PDC state (dotted black lines) to a correlated PDC state (green, purple or solid black lines) . Left: JSA. Center: reduced density matrix of signal. Right: HOM dip between signal and reference. Both cases, correlated and uncorrelated, have the same marginal spectral widths. Nevertheless, the width of the HOM dip reveals the amount of correlations.

Joint spectral intensity and second order correlation function Alternatively to HOM interference measurements, information about the separability of the state can be inferred from the joint spectral intensity (JSI) $|f(\omega_s, \omega_i)|^2$ or the second order Glauber correlation function $g^{(2)}(\tau)$ [33] of the signal or idler field without heralding on a photon in the opposite mode. The $g^{(2)}(0)$ value gives information about the photon number statistics of the marginal beams. For a decorrelated PDC state, the marginal statistics are thermal with $g^{(2)}(0) = 2$ and for a strongly correlated state, the marginal statistics are Poissonian with $g^{(2)}(0) = 1$ [16]. The relation between the Schmidt number and the marginal Glauber correlation function is given by $g^{(2)}(0) = 1 + 1/K$ [19, 34].

All three methods for source characterization have already been applied in the literature. However, there is no ideal measurement: A JSI measurement is affected by a low spectral resolution and cannot resolve correlations hidden in the phase of the JSA. Furthermore, it is blind to any non spectral correlations. A $g^{(2)}(0)$ measurement is sensitive to correlations in all degrees of freedom, but is, unfortunately, strongly affected by detector dark counts and non-PDC background signal. The HOM interference measurement requires the exact knowledge of spectral widths of signal and reference fields. Therefore it makes sense to apply all three techniques and carefully compare their results as we do in this paper.

3. Experimental results

3.1. Experimental setup

We employ type-II PDC in ppKTP waveguides. At telecom wavelength it offers a positively correlated phasematching function with a correlation angle of 59 degrees, such that a decorrelated JSA can be produced using the correct pump width [19]. Such waveguides can be routinely produced and are commercially available. Our chip is purchased from ADVR and has the following parameters: a length of 8 mm, waveguide dimensions of about $4\,\mu\text{m} \times 6\,\mu\text{m}$ and a poling

period of $117\,\mu$m.

A scheme of the setup is shown in Fig. 4. It consists of a Ti:Sapph pumped OPO (Chameleon Compact OPO) running at 80 MHz and producing short pulses of 250 fs at 1536 nm. A small part of the light is separated for the reference beam while the major part is frequency doubled in a BBO crystal. The cascade of Ti:Sapph, OPO and SHG is necessary to achieve a good synchronization between the coherent reference beam and the PDC light. A crucial part of the experiment is the spectral shaping of the pump. We employ a $4f$-spectrometer, consisting of two gratings, two lenses and one slit in the center, all separated by the focal length of the lenses. The width of the spectrum can be narrowed by reducing the width of the slit. Additionally, the slit is tilted, effectively reducing the resolution of the spectrometer, to produce Gaussian spectral shapes rather than square-like shapes. The spectrum of both, pump and reference beams, is measured and monitored by an optical spectrum analyzer (OSA).

We use aspheric lenses for in- and outcoupling of the waveguide and the fibers. Behind the waveguide, we employ a longpass filter (Semrock LP02-808RU-25) to block out the pump beam and a bandpass filter (Semrock NIR01-1535/3-25) with an FWHM of 8 nm. This bandpass filter is the second crucial part of the experiment because the PDC generates background signal over a wide spectral range [35]. The bandpass filter is chosen such that it blocks as much background signal as possible without affecting the PDC signal itself. All beams are coupled into single mode fibers (SMF). For the detection at the single photon level, we use avalanche photo diodes (APDs) (either Id Quantique id201 or NuCrypt CPDS-1000-4). The repetition rate of the id201 is 1 MHz and of the CPDS-1000-4 40 MHz. We measure raw coincidence vs single ratios, i.e. Klyshko efficiencies [36–38] of up to 20.5% for the signal beam and 15.5% for the idler beam. Corrected for the detector (id201) efficiencies of approximately 25% and 22%, these values correspond to coupling efficiencies into the SMFs of roughly 80% in one arm and 70% in the other arm, making our source highly compatible with existing fiber based telecommunication technologies.
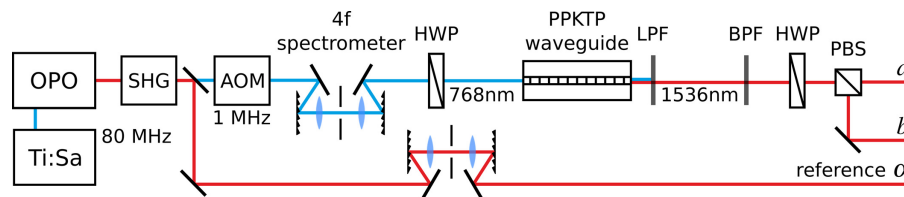

Fig. 4. Scheme of the setup. Pulsed light at telecom wavelengths is generated in an Ti:Sapph pumped optical parametric oscillator (OPO) and frequency doubled by second harmonic generation (SHG). Part of the light is separated for later use as a reference field. The repetition rate is lowered by an acousto-optical modulator (AOM) to match the repetition rate of the gated APDs. The 4-f spectrometer tailors the spectral width of the pump beam to achieve spectral decorrelation. The PDC state is generated inside the periodically poled KTP waveguide. The pump is separated by a long pass filter (LPF). A bandpass filter (BPF) is used to suppress background outside the PDC spectrum. Finally signal and idler are separated at a polarizing beam splitter (PBS).

3.2. Spectral measurements

We characterize the spectral properties of our source with a fiber spectrometer [39] (see first frame of Fig. 5). Signal and idler travel through dispersive fibers before impinging onto two APDs. Different wavelengths arrive at different times. By scanning the gating times of the APDs, a joint spectral intensity (JSI) distribution is obtained from coincidence click rates. Sim-
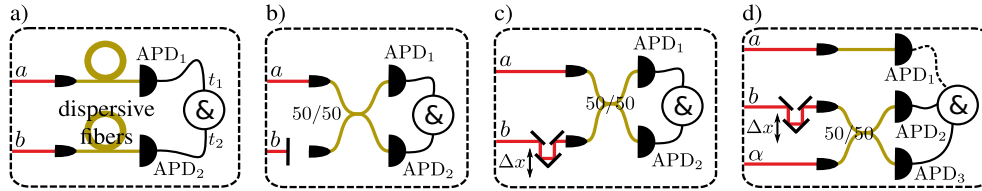
Fig. 5. Scheme of different measurement settings. a) JSI measurement; b) $g^{(2)}(0)$ measurement; c) HOM interference between signal and idler; d) 2-fold or 3-fold HOM interference with a reference field. The Id Quantique detectors(1 MHz) are used for the JSI measurement and the NuCrypt detectors (40 MHz) for the rest.

ilarly, the marginal spectral distribution of signal and idler are obtained from the single click rates. The resolution of the fiber spectrometer is limited by the gate width of the APDs and the length of the fiber. We use the id201 with a gate width of approximately 1.5 ns, resulting in a spectral resolution of 1.8 nm for the JSI and 0.9 nm for the marginal spectra.

The JSI and the marginal spectral distributions with and without the bandpass filter are shown in fig. 6. The bandpass filter has a width of 8 nm and one can see from the comparison of the unfiltered with the filtered spectrum in Fig. 6 that background signal is suppressed directly outside of the PDC range while the PDC spectrum itself is mostly unaffected. The spectra of signal and idler have Gaussian shapes and their widths at FWHM, obtained from Gaussian fits, are 5.2 nm and 4.0 nm, respectively. Assuming that the finite resolution is effectively a convolution with an 0.9 nm wide Gaussian, the true widths can be estimated to be 5.1 nm and 3.9 nm. The theoretical sinc-shape of the spectrum is smeared out by experimental imperfections of the waveguide structure. The congruence of the data points with the fit curve supports the assumption of a Gaussian JSA in Sec. 2.2.

The JSI measurement in the decorrelated case shows a smooth, nearly round shape. This also supports the assumption of Gaussian phasematching and pump spectral profiles. Being an intensity distribution, the JSI does not provide full information about the state as additional phase or temporal information would be required to reconstruct the JSA [40]. A singular value decomposition of the square root of the JSI, yielding an effective mode number of 1.001 in our case, can therefore be only regarded as a lower bound for the true Schmidt number.

To obtain a stronger statement about the correlations present in the source, we measure the second order Glauber correlation function $g^{(2)}(0)$ with a 50/50 fiber coupler [16], as depicted in the second frame of Fig. 5. We find raw values of 1.83 ± 0.02 and 1.86 ± 0.02 for signal and idler, respectively. These values pose an upper bound on the correlations present in the PDC source. The corresponding Schmidt numbers are 1.20 and 1.16. Part of the deviation from the perfectly decorrelated case could be caused by background events. From comparison of the filtered with the unfiltered spectra, we conclude that the background still remaining under the PDC spectrum makes up for approximately 1.9 % of the total count rates. Since background signal has a Poissonian photon number distribution, it strongly degrades the $g^{(2)}(0)$ value. Correcting for these background events [35], we get values of 1.90 and 1.94. However, we would like to note that the raw value of $g^{(2)}(0) = 1.86$ is among the highest compared to other PDC sources [16, 19, 41, 42] indicating that the amount of background events is relatively low.

3.3. Interference measurements

To demonstrate the indistinguishability between signal and idler, we interfere them at a 50/50 fiber coupler, as sketched in the third frame of Fig. 5. The coincidence rate versus a delay of one
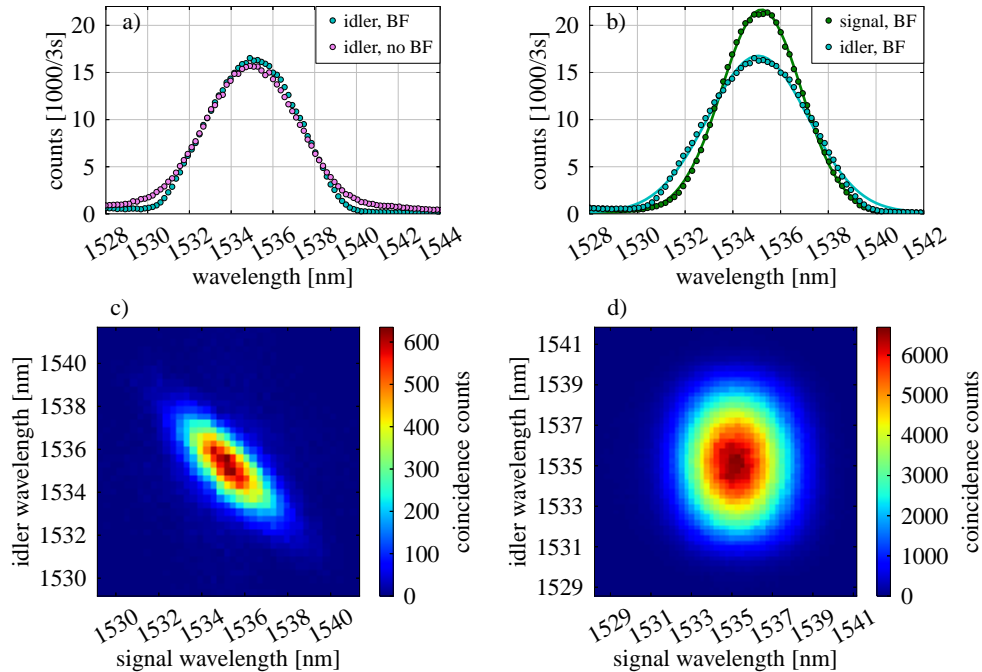
Fig. 6. a) Marginal idler spectra for the decorrelated case with and without the bandpass filter (BF). One can see that the spectral filter fits nicely the idler spectrum, touching it only slightly at the very edges. b) Signal and idler spectra with the bandpass filter. Bottom: Measured joint spectral intensity for anticorrelation (c) and decorrelation (d). The pump widths are 0.5 nm and 2.1 nm, respectively.

of the beams is shown in Fig. 7. The measurement is done with a pump energy as low as 0.6 pJ per pulse leading to a mean photon number of 0.002. We obtain a visibility of $(94.8 \pm 0.6)\%$, which is to our knowledge the highest value reported in the literature for PDC sources without narrowband filtering. It is close to the theoretical value of 96.7% for the decorrelated case. Part of that small deviation from the theoretical value is caused by our fiber coupler which has a slightly uneven coupling ratio of 49.1/50.9. The high visibility of the interference shows that the indistinguishability between signal and idler is indeed very high.

As discussed in the theory section, a robust method for verifying the decorrelation of the PDC state is to measure the purity of the marginal beams by HOM interference with a reference field. As the reference field, we use part of the original laser beam and attenuate it to the single photon level. All three beams, signal, idler and reference are coupled into single mode fibers and the count rates are recorded with the APDs, as sketched in Fig. 5. We record two-fold and three-fold coincidences, where by two-fold we mean coincidence events behind the beam splitter disregarding the third APD and by three-fold we mean triple coincidences between all three output ports. The heralding with the second PDC beam in the three-fold case increases the visibility of the interference [8]. The results are shown in Fig. 8. As expected, the visibility in the three-fold case is higher than in the two-fold case. It depends on the spectral overlap between the two beams as well as the mean photon numbers which for this measurement are 0.006 for the marginal beam and 0.08 for the reference beam. For calculating the purity of the state, we use the width of the dip rather than the visibility. Both two-fold and three-fold curves have similar widths of 1.33 ± 0.02 ps and 1.28 ± 0.04 ps. Taking into account the spectral width
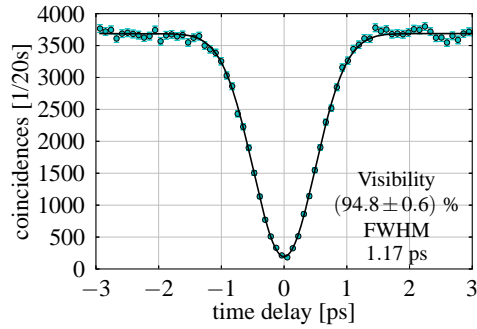
Fig. 7. HOM interference between signal and idler.

of the Gaussian reference field of 4.5 nm and the signal spectral width of 3.9 nm, we calculate a purity of $82.1 \pm 1.7\%$ and $86.7 \pm 4.3\%$. These values are in good agreement with the raw $g^{(2)}(0)$ values. Compared to other PDC sources without narrowband filtering, Mosley et. al [18] have shown higher purities around 95% by measuring the HOM interference between two independent PDC sources. Our measured purities are slightly below this value but still in the same range, demonstrating excellent source performance. Similar values have been obtained in [43], who also utilized HOM interference with a coherent field.
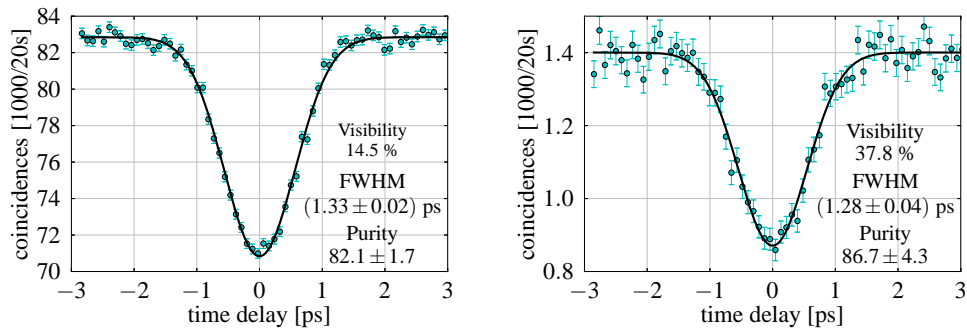

Fig. 8. two-fold (left) and three-fold (right) HOM interference between signal and reference.

3.4. Source brightness

In the low power regime at which the above interference measurements are performed, we measure a photon pair generation efficiency of 3×10^9 (photon pairs)/J or 3.8×10^{11} (photon pairs)/(J $\times$ m), if taken per unit crystal length and pump energy. Taking into account that all photons are generated in a single mode, the source brightness is extremely high, even for low pump powers. For a mean photon number per pulse of 0.1 in the signal beam, the required cw equivalent power at a repetition rate of 1 MHz is only 33 μW. By using the full available power in our setup of 2.5 mW (2.5 nJ per pulse), we are able to reach a mean photon number of approximately 80 photon pairs per pulse. This high number is due to the single mode character of our source and much higher than is expected for a multimode source with the same photon pair generation efficiency.

4. Conclusion

In conclusion, we have implemented a source with remarkable properties in terms of brightness, purity and symmetry. The HOM interference between signal and idler showed, to our knowledge, an unprecedented visibility of 94.8%. The purity values for signal and idler obtained from $g^{(2)}$, JSI and interference with a reference beam reveal a purity of above 80%. In order to reach a desirable mean photon number around 0.1 photon pairs per pulse, pump energies as low as 33 pJ are required, which significantly simplifies the simultaneous operation of several sources. Our source can be easily combined with identical sources or other optical fields and constitutes a step towards the feasibility of more complex quantum circuits or networks.

Acknowledgement